Cancellation of the polarization distortions in fiber-based polarization-sensitive Mueller-matrix optical coherence tomography

Shuliang Jiao, Wurong Yu, George Stoica, Lihong V. Wang

Shuliang Jiao, Wurong Yu, George Stoica, Lihong V. Wang, "Cancellation of the polarization distortions in fiber-based polarization-sensitive Mueller-matrix optical coherence tomography," Proc. SPIE 4956, Coherence Domain Optical Methods and Optical Coherence Tomography in Biomedicine VII, (8 July 2003); doi: 10.1117/12.479033

SPIE.

Event: Biomedical Optics, 2003, San Jose, CA, United States

Cancellation of the polarization distortions in fiber-based polarization-sensitive Mueller-matrix optical coherence tomography

Shuliang Jiao[a], Wurong Yu[a], George Stoica[b], and Lihong V. Wang[a*]
[a]Optical Imaging Laboratory, Department of Biomedical Engineering,
Texas A&M University, 3120 TAMU, College Station, TX 77843-3120
[b]Department of Pathobiology, Texas A&M University, College Station, TX 77843-5547

ABSTRACT

A multi-channel polarization-sensitive Mueller-matrix optical coherence tomography (OCT) was built with single-mode optical fibers in both the sample and reference arms. A new rigorous algorithm was developed to eliminate dynamically the polarization distortions caused by the sampling fiber and consequently retrieve the calibrated polarization properties of the sample. The roundtrip Jones matrix of the sampling fiber used in the algorithm was acquired from the reflecting surface of the sample for each depth scan (A scan). Both this new algorithm and the algorithm used in previous fiber-based polarization-sensitive OCT (PS-OCT) were tested with simulated data, which shows that the only parameter that can be correctly retrieved by the previous algorithm is the phase retardation. The skin of a rat was imaged with this fiber-based system.
Keywords: optical coherence tomography, Mueller matrix, Jones matrix, polarization, optical fiber

1. INTRODUCTION

As an important branch of optical coherence tomography (OCT), polarization-sensitive OCT (PS-OCT) adds the polarization properties of the sample as a contrast mechanism.[1–8] However, practical applications of PS-OCT have been limited by the difficulty of its optical-fiber implementation. A single-mode optical fiber (SMF) alters the polarization state of the guided light wave due to the inherent birefringence in the fiber, which exists when the cylindrical symmetry of its core is broken by factors such as stress. The birefringence varies with the bending and twisting of the fiber during manipulation of the imaging probes, which can result in dynamic distortion in PS-OCT images. Therefore, a dynamic calibration technique is required to eliminate this effect.

Based on previous studies, a Jones matrix can be applied in PS-OCT to completely characterize the polarization properties of an optical element and a scattering medium.[4–8] If the one-way Jones or Mueller matrix of the sampling optical fiber can be determined, the polarization distortion caused by the sampling fiber can be eliminated from the PS-OCT images. Multi-channel Mueller OCT can measure the Jones and Mueller matrices of a sample with a single scan and thus offer the possibility of rigorously eliminating the polarization effect of the sampling fiber. This method allows fiber-based Mueller OCT to acquire a calibrated Mueller-matrix image as rapidly as conventional OCT acquires a regular image. In this paper, we report a new rigorous algorithm for the retrieval of the calibrated polarization properties of the sample. This algorithm was validated with simulated data. The skin of a rat was imaged as well.

2. CALIBRATION ALGORITHM

In general, a pure retarder can be characterized by a homogeneous Jones matrix that has two orthogonal elliptical eigen-vectors, each representing an eigen-polarization. A linear retarder is a special case where the eigen-polarizations are linear; and a Faraday rotator is another special case where the eigen-polarizations are circular. When two or more linear retarders are cascaded, the overall retarder is generally elliptical unless the axes are aligned. Due to its randomly distributed birefringence along the core, a SMF should be treated as an elliptical retarder.

* To whom all correspondence should be addressed. Tel: 979-847-9040; Fax: 979-845-4450; Email: LWang@tamu.edu; URL: http://oilab.tamu.edu.

Coherence Domain Optical Methods and Optical Coherence Tomography in Biomedicine VII,
Valery V. Tuchin, Joseph A. Izatt, James G. Fujimoto, Editors, Proceedings of SPIE
Vol. 4956 (2003) © 2003 SPIE · 1605-7422/03/$15.00

We first introduce the general properties of a retarder. The 2×2 Jones matrix [$\mathbf{J}(\varphi,\theta,\delta)$] of an elliptical retarder can be expressed with three independent real parameters:

$$\mathbf{J}(\varphi,\theta,\delta)=\begin{bmatrix} e^{i\varphi/2}\cos^2\theta+e^{-i\varphi/2}\sin^2\theta & (e^{i\varphi/2}-e^{-i\varphi/2})\sin\theta\cos\theta e^{-i\delta} \\ (e^{i\varphi/2}-e^{-i\varphi/2})\sin\theta\cos\theta e^{i\delta} & e^{i\varphi/2}\sin^2\theta+e^{-i\varphi/2}\cos^2\theta \end{bmatrix} \tag{1}$$

$$J(2,1)=-J^*(1,2),\ J(2,2)=J^*(1,1).$$

The fast and slow eigen-vectors are $\begin{bmatrix}\cos\theta \\ \sin\theta\exp(i\delta)\end{bmatrix}$ and $\begin{bmatrix}-\sin\theta\exp(-i\delta) \\ \cos\theta\end{bmatrix}$, respectively. The angle θ is an auxiliary angle of the fast eigen-vector; δ represents the phase difference between the two components of the fast eigen-vector; and φ is the phase difference (retardation) between the two eigen-values. If δ = 0, the retarder is linear and θ represents the orientation of the fast axis.

The roundtrip Jones matrix ($\mathbf{J}_2$) of an optical component can be calculated from its one-way Jones matrix ($\mathbf{J}_1$) according to the Jones reversibility theorem:

$$\mathbf{J}_2=\mathbf{J}_1^T\mathbf{J}_1. \tag{2}$$

Subscripts 1 and 2 denote the one-way and roundtrip parameters, respectively. Because $\mathbf{J}_2$ is transpose symmetric [$J_2(2,1)=J_2(1,2)$], the phase difference δ_2 of $\mathbf{J}_2$ is zero, indicating $\mathbf{J}_2$ represents a linear retarder. As a result, only two independent real parameters are needed to describe $\mathbf{J}_2$.

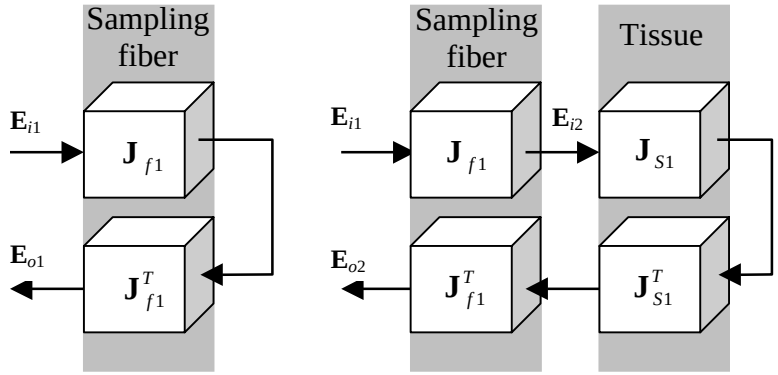

Fig. 1 Illustration of the polarization transformation in the sample arm. $\mathbf{E}_{i1}$ and $\mathbf{E}_{i2}$: incident Jones vectors for the sampling fiber and the sample; $\mathbf{E}_{o1}$: the measured output roundtrip Jones vector from the sample surface; $\mathbf{E}_{o2}$: the roundtrip Jones vector representing the transformation result of both the fiber and the tissue layer; $\mathbf{J}_{f1}$ and $\mathbf{J}_{s1}$: the one-way Jones matrix of the sampling fiber and the sample.

As shown in Fig. 1, in a fiber-based Mueller OCT system, the incident sampling light undergoes transformation sequentially, first through the sampling fiber and the sample in forward propagation and then the sample and the sampling fiber in backward propagation. Therefore, the raw roundtrip Jones matrix ($\mathbf{J}_{sf2}$) can be expressed in terms of the one-way Jones matrix of the sampling fiber ($\mathbf{J}_{f1}$) and the roundtrip Jones matrix of the sample at a given imaging depth ($\mathbf{J}_{s2}$) as

$$\mathbf{J}_{sf2}=\mathbf{J}_{f1}^T\mathbf{J}_{s2}\mathbf{J}_{f1}. \tag{3}$$

The roundtrip Jones matrix of the sampling fiber ($\mathbf{J}_{f2}$) can be calculated from the OCT signal reflected from the sample surface:

$$\mathbf{J}_{f2}=\mathbf{J}_{f1}^T\mathbf{J}_{f1}. \tag{4}$$

To eliminate the distortion, the best approach is to calculate $\mathbf{J}_{f1}$ from $\mathbf{J}_{f2}$ for each A scan. However, there are three real variables in $\mathbf{J}_{f1}(\varphi_{f1}, \theta_{f1}, \delta_{f1})$ but only two in $\mathbf{J}_{f2}(\varphi_{f2}, \theta_{f2})$. Consequently, Eq. (4) provides only two independent relationships; therefore, $\mathbf{J}_{f1}$ can only be determined from $\mathbf{J}_{f2}$ with a free parameter.

For each $\mathbf{J}_{f2}$, we can always find a unique hypothetical linear retarder $\mathbf{J}_{fl1}$ to satisfy

$$\mathbf{J}_{f2} = \mathbf{J}_{fl1}^{T} \mathbf{J}_{fl1}. \tag{5}$$

We introduce the following matrix to reflect the free parameter:

$$\mathbf{J}_{fc1} = \mathbf{J}_{f1} \mathbf{J}_{fl1}^{-1}. \tag{6}$$

Removing the round-trip effect of $\mathbf{J}_{fl1}$ from $\mathbf{J}_{sf2}$, we obtain a new matrix $\mathbf{J}_{sc2}$:

$$\mathbf{J}_{sc2} = (\mathbf{J}_{fl1}^{T})^{-1} \mathbf{J}_{sf2} \mathbf{J}_{fl1}^{-1}. \tag{7}$$

Based on Eqs. (3)–(7), we have the following solution representing the general calibration algorithm in a matrix form:

$$\mathbf{J}_{s2} = (\mathbf{J}_{fc1}^{T})^{-1} \mathbf{J}_{sc2} \mathbf{J}_{fc1}^{-1}. \tag{8}$$

The round-trip retardation (φ_{s2}) of the sample can be calculated by[9]

$$\varphi_{s2} = 2\cos^{-1}\left\{\frac{1}{2}\frac{\left|\mathrm{tr}\,\mathbf{J}_{s2} + \det \mathbf{J}_{s2} / \left|\det \mathbf{J}_{s2}\right| \mathrm{tr}\,\mathbf{J}_{s2}^{*}\right|}{[\mathrm{tr}(\mathbf{J}_{s2}^{*}\mathbf{J}_{s2}) + 2\left|\det \mathbf{J}_{s2}\right|]^{1/2}}\right\}, \tag{9}$$

or, in the case of negligible diattenuation in the sample, by

$$\varphi_{s2} = 2\cos^{-1}\{[J_{s2}(1,1) + J_{s2}(2,2)]/2\}. \tag{10}$$

We can also prove from Eq. (6) that the elements of $\mathbf{J}_{fc1}$ are real numbers and that $J_{fc1}^{2}(1,1) + J_{fc1}^{2}(1,2) = 1$. Consequently, we can introduce a new parameter γ as follows:

$$\mathbf{J}_{fc1} = \begin{bmatrix} \cos\gamma & \sin\gamma \\ -\sin\gamma & \cos\gamma \end{bmatrix}. \tag{11}$$

$\mathbf{J}_{fc1}$ thus represents a rotation matrix. In other words, the Jones matrix of the sampling fiber is decomposed into a linear retarder and a rotator. Equation (8) is equivalent to rotating the fast axis of $\mathbf{J}_{s2}$ along the axis of the incident light by an angle γ. This rotation does not affect the amplitudes of either the birefringence or diattenuation. As a result, the calibrated round-trip retardation of the sample can be calculated exactly from Eq. (9). From Eqs. (8) and (11), we can calculate the calibrated orientation of birefringence as follows:

$$\theta_{s2} = \theta_{sc2} - \gamma, \tag{12}$$

where θ_{sc2} can be calculated from the fast eigenvector of $\mathbf{J}_{sc2}$.

The calibration in Eq. (12) has an offset γ, which depends on the parameters of the sampling fiber only. This offset is a constant in a frame of image as long as the parameters of the sampling fiber are kept constant during the image acquisition of each frame, which is the case when the fast lateral scanning of OCT does not move the sampling fiber. Therefore, a relative distribution of the orientation of the birefringence can be retrieved. If the parameters of the sampling fiber are varied among the A scans, which is true when the lateral scanning in OCT does move the sampling fiber, γ will differ among the A lines. In this case, if the orientation of the birefringence of the surface layer is constant

or known *a priori*, or if a known thin retarder is attached to the sample as the first layer, γ can be eliminated. In either case, φ_{s2} can be calculated exactly.

We tested the algorithm for a simulated fiber with parameters $\varphi_{f1} = 46^\circ, 0 \le \theta_{f1} < \pi,\ 0 \le \delta_{f1} < \pi$ and $0 < \varphi_{f1} < \pi,\ 0 \le \theta_{f1} < \pi,\ \delta_{f1} = 50^\circ$, respectively, together with a sample having various parameters of birefringence. The birefringent parameters of the simulated sample can be completely recovered. Fig. 2 shows the simulation results with $\varphi_{s2} = 36^\circ$.

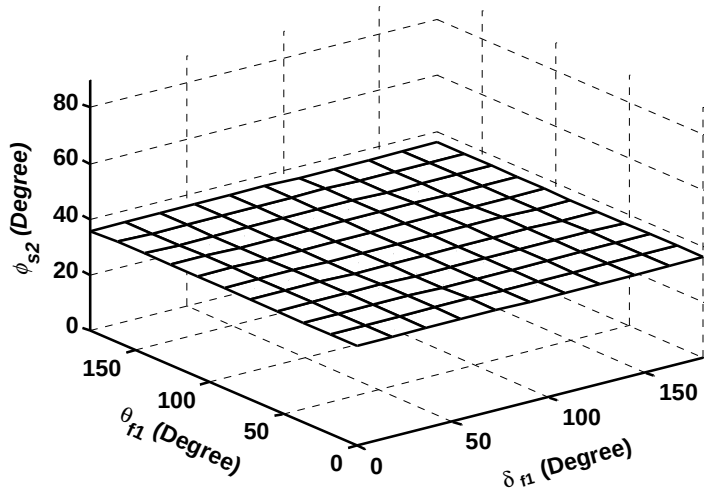

(a)

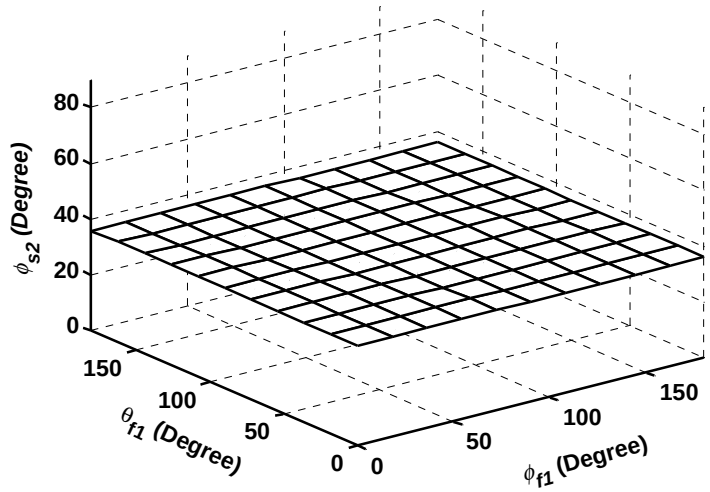

(b)

Fig. 2 The calibration results for a simulated sample with $\varphi_{s2} = 36^\circ$ and sampling-fiber parameters: (a) $\varphi_{f1} = 46^\circ; 0 \le \theta_{f1} < \pi;\ 0 \le \delta_{f1} < \pi$ and (b) $\delta_{f1} = 50^\circ; 0 \le \theta_{f1} < \pi;\ 0 \le \varphi_{f1} < \pi$.

3. COMPARISON OF THE ALGORITHM WITH CONVENTIONAL PS-OCT

In this section, we compare the above algorithm for eliminating the polarization distortions of the sampling fiber with the a previous algorithm used in conventional fiber-based PS-OCT.[10] As illustrated in Fig. 1, we have the following relations:

$$\mathbf{E}_{i2} = \mathbf{J}_{f1}\mathbf{E}_{i1}, \tag{13}$$

$$\mathbf{E}_{o1} = \mathbf{J}_{f1}^{T}\mathbf{J}_{f1}\mathbf{E}_{i1}, \tag{14}$$

$$\mathbf{E}_{o2} = \mathbf{J}_{f1}^{T}\mathbf{J}_{s2}\mathbf{J}_{f1}\mathbf{E}_{i1}. \tag{15}$$

Each of the Jones vectors $\mathbf{E}_{i1}$, $\mathbf{E}_{i2}$, $\mathbf{E}_{o1}$, and $\mathbf{E}_{o2}$ has a corresponding Stokes vector $\mathbf{S}_{i1}$, $\mathbf{S}_{i2}$, $\mathbf{S}_{o1}$ and $\mathbf{S}_{o2}$, respectively. In the algorithm developed in Ref. 10, a rotation matrix was calculated to transform $\mathbf{S}_{o1}$ to $\mathbf{S}_{o2}$ in the Poincare sphere in the effort to calculate the polarization parameters of the sample. The rotation matrix is considered to represent a pure retarder. Because Jones and Mueller calculus are equivalent in PS-OCT and Poincare sphere just represents the visualization of Mueller calculus, we use Jones calculus for its simplicity to examine the effect of the algorithm in Ref. 10 on the calculated polarization parameters of the sample.

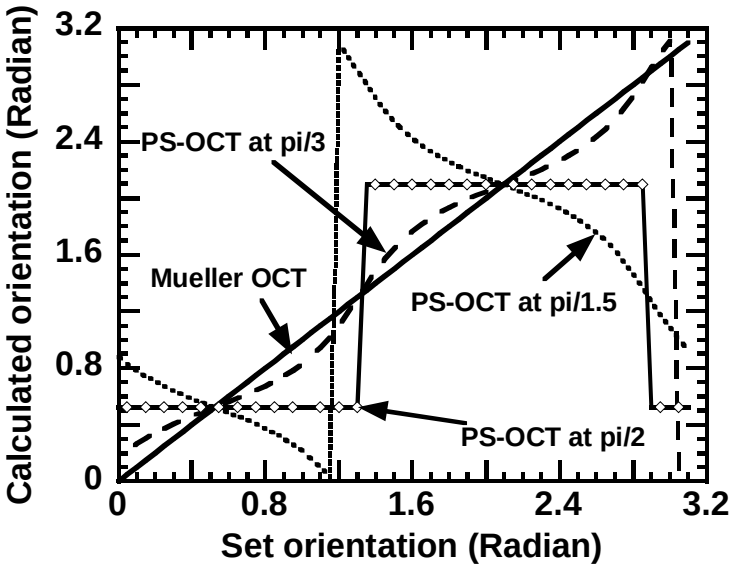

Fig. 3 The calculated orientation of the fast axis with the two different algorithms for a fiber-based PS-OCT system

From Eq. (6), we can see that the one-way Jones matrix of the sampling fiber can be decomposed into the product of a linear retarder and a rotator:

$$\mathbf{J}_{f1} = \mathbf{J}_{fc1}\mathbf{J}_{fl1}. \tag{16}$$

Eq. (14) becomes

$$\mathbf{E}_{o1} = \mathbf{J}_{fl1}^{T}\mathbf{J}_{fc1}^{T}\mathbf{J}_{fc1}\mathbf{J}_{fl1}\mathbf{E}_{i1} = \mathbf{J}_{fl1}^{T}\mathbf{J}_{fl1}\mathbf{E}_{i1}, \tag{17}$$

and we have

$$\mathbf{J}_{fl1}\mathbf{E}_{i1} = \mathbf{J}_{fl1}^{-1}\mathbf{E}_{o1}. \tag{18}$$

We can then represent $\mathbf{E}_{o2}$ with $\mathbf{E}_{o1}$ by inserting Eq. (18) into Eq. (15):

$$\begin{aligned}\mathbf{E}_{o2} &= \mathbf{J}_{fl1}^{T}\mathbf{J}_{fc1}^{T}\mathbf{J}_{s2}\mathbf{J}_{fc1}\mathbf{J}_{fl1}^{-1}\mathbf{E}_{o1} \\ &= (\mathbf{J}_{fl1}\mathbf{J}_{fc1}^{-1})\mathbf{J}_{s2}(\mathbf{J}_{fl1}\mathbf{J}_{fc1}^{-1})^{-1}\mathbf{E}_{o1}\,. \\ &\neq \mathbf{J}_{s2}\mathbf{J}_{f2}\mathbf{E}_{01}\end{aligned} \tag{19}$$

The transformation matrix $(\mathbf{J}_{fl1}\mathbf{J}_{fc1}^{-1})\mathbf{J}_{s2}(\mathbf{J}_{fl1}\mathbf{J}_{fc1}^{-1})^{-1}$ in Eq. (19) is the representation in the Jones calculus of the calculated rotation matrix by the algorithm in Ref. 10. This matrix is generally an elliptical retarder and is not identical to what we are after, i.e., the roundtrip Jones matrix of the tissue: $\mathbf{J}_{s2}$. We can prove that the retardation of $(\mathbf{J}_{fl1}\mathbf{J}_{fc1}^{-1})\mathbf{J}_{s2}(\mathbf{J}_{fl1}\mathbf{J}_{fc1}^{-1})^{-1}$ happens to be equal to the retardation of $\mathbf{J}_{s2}$, but the orientation has a complicated nonlinear relationship with the orientation of $\mathbf{J}_{s2}$.

When the fiber can be characterized as a linear retarder, $\mathbf{J}_{fc1}$ becomes an identity matrix and Eq. (19) becomes:

$$\mathbf{E}_{o2} = \mathbf{J}_{fl1}\mathbf{J}_{s2}\mathbf{J}_{fl1}^{-1}\mathbf{E}_{o1} \neq \mathbf{J}_{s2}\mathbf{E}_{o1}\,. \tag{20}$$

The transformation matrix $\mathbf{J}_{fl1}\mathbf{J}_{s2}\mathbf{J}_{fl1}^{-1}$ still represents an elliptical element and is not the desired matrix $\mathbf{J}_{s2}$.

Another aspect we must notice is that this algorithm is not valid when diattenuation exists in a sample because the rotation of the Stokes vector from $\mathbf{S}_{o1}$ to $\mathbf{S}_{o2}$ is assumed to be caused only by birefringence. As a result, we regard conventional fiber-based PS-OCT as a single-parameter PS-OCT system, which can reveal the amplitude of birefringence only.

The orientation of the fast axis of the transformation matrix in Eq. (19) was calculated for a system whose sampling fiber can be considered as a linear retarder with one-way retardation $\varphi_{f1} = \pi/3, \pi/2, \pi/1.5$ and orientation $\theta_{f1} = \pi/6$. The roundtrip retardation of the sample is $\varphi_2 = \pi/3$, and its orientation changes from 0 to π. The calculation results are shown in the Fig. 3. For comparison, the orientation of the fast axis of the sample extracted with the algorithm of Mueller OCT is also shown in the figure. We draw the following conclusions:

1). The algorithm of the Mueller OCT is stable and yields exact orientation of the fast axis of the sample in the entire data range.

2). Without discriminating the one-way and roundtrip transformation effects, the algorithm used in conventional fiber-based PS-OCT is unable to consider the actual order of transformation. As a result, the calculated orientation of the fast axis of the sample is wrong except at two points--when the orientations of the fiber and the sample are either parallel or orthogonal. With an increase of retardation in the sampling fiber, the error becomes more severe.

4. Experimental Setup

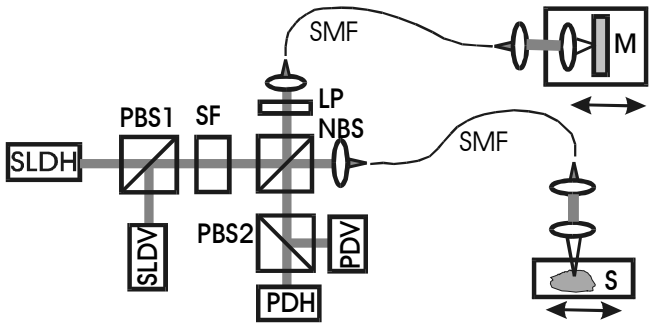

Fig. 4 Schematic of the fiber-based Mueller OCT system. SLDH and SLDV: superluminescent diodes, horizontally polarized (*H*) and vertically polarized (*V*), respectively; PBS1 and PBS2: polarizing beam splitters; SF: spatial filter assembly; NBS: non-polarizing beam splitter; M: mirror; SMF: single-mode optical fiber; PDH and PDV: photodiodes for the *H* and *V* polarization components, respectively.

Fig. 4 shows a schematic of the experimental system. The two source beams from two SLD sources (central wavelength $\overline{\lambda}$ = 850 nm, FWHM bandwidth $\Delta\lambda$ = 26 nm), amplitude-modulated at 3 kHz and 3.5 kHz, respectively, are merged by a polarizing beam splitter (PBS1), filtered by a spatial-filter, and then split by a non-polarizing beam splitter (NBS). Both the sample and the reference beams are coupled into a 0.5-m long SMF, respectively. A 45° linear polarizer (LP) is used to control the polarization state of the reference beam. The combined backscattered and reference light is split into the horizontally (*H*) and vertically (*V*) polarized components by a polarizing beam splitter PBS2; these are detected by photodiodes PDH and PDV, respectively. The data processing and the Jones matrix calculation have been described in our previous works.[6,7]

5. RESULTS AND DISCUSSION

We first tested the system by imaging a quarter-wave ($\lambda/4$) plate in combination with a mirror, for a frame consisting of 35 A scans with a lateral span of 1 mm. The sampling fiber was intentionally deformed every fifth A scan to vary its polarization property. The measured $\mathbf{J}_{f2}$ was used to cancel the distortion using the above algorithm. The calibrated φ_{s2} of the $\lambda/4$ plate accurately matches the expected value of $\lambda/2$, indicating the validity of our algorithm.

The fiber-based Mueller OCT system was used to image a biological sample—the skin of a rat tail [Berlin Drucrey (BD-IV)] *in vivo*. After the rat was anesthetized (ketamine 60 mg/kg, IM) and the hair of the tail was removed with hair remover lotion, the tail was scrubbed with glycerin. Two-dimensional data of the skin were taken by laterally moving the sample between A scans. The Jones matrix was calibrated pixel-wise to eliminate the fiber distortions and then converted into its corresponding 4×4 Mueller matrix. Polarization parameters of the sample were extracted from the Jones or Mueller matrix. Fig. 5 shows the images of the polarization-independent M_{00} element of the Mueller matrix, the amplitude of retardation after calibration, and the orientation of the fast axis. Some structures, like the epidermis and the collagen-rich dermal papillae, can be clearly seen in the M_{00} and retardation images. Also shown in Fig. 5 is the haematoxylin and eosin (*HE*) histological image of the tail skin of the same breed. The calibrated OCT images conform well with the histological image.

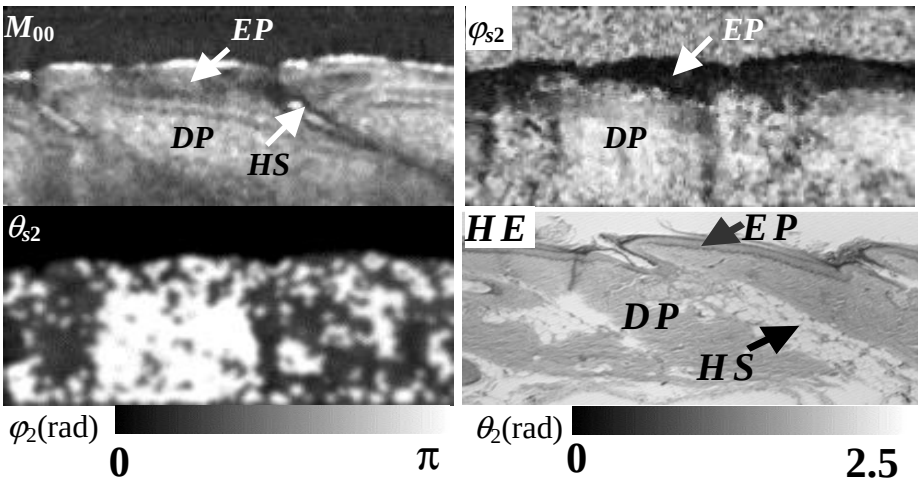

Fig. 5 The M_{00} image of the Mueller matrix, the calculated retardation image φ_{s2}, and the image of the orientation of the fast axis of the skin of a rat tail measured *in vivo* with the fiber-based Mueller OCT system. The M_{00} image is in logarithmic scale while the retardation image is in linear scale. The height of the images is 1mm. *EP*: Epidermis; *DP*: dermal papilla; *HS*: hair shaft.

5. CONCLUSION

In conclusion, single-mode optical fibers were successfully incorporated into our Mueller OCT system. A rigorous algorithm was invented to exactly eliminate the polarization effect of the sampling fiber on the retardation image of a

sample dynamically. With this algorithm, the distribution of the orientation of the birefringence can also be extracted with only a constant offset in each pixel as long as the sampling fiber is not scanned during the acquisition of each frame of image. Our fiber-based Mueller OCT system was successfully applied to imaging biological samples.

ACKNOWLEDGEMENTS

This project was sponsored in part by National Institutes of Health grants R21 EB00319-02 and R01 EB000712, by National Science Foundation grant BES-9734491, and by Texas Higher Education Coordinating Board grant 000512-0063-2001.

REFERENCE

1. J. F. de Boer, T. E. Milner, M. J. C. van Gemert and J. S. Nelson, "Two-dimensional birefringence imaging in biological tissue by polarization-sensitive optical coherence tomography", *Opt. Lett*. **22**, 934–936 (1997).
2. M. J. Everett, K. Schoenerberger, B. W. Colston, Jr., L. B. Da Silva, "Birefringence characterization of biological tissue by use of optical coherence tomography", *Opt. Lett*. **23**, 228–230 (1998).
3. J. F. de Boer, T. E. Milner, and J. S. Nelson, "Determination of the depth-resolved Stokes parameters of light backscattered from turbid media by use of polarization-sensitive optical coherence tomography", *Opt. Lett*. **24**, 300–302 (1999).
4. G. Yao and L.-H. V. Wang, "Two-dimensional depth-resolved Mueller matrix characterization of biological tissue by optical coherence tomography", *Opt. Lett*. **24**, 537–539 (1999).
5. S. Jiao, G. Yao and L.-H. V. Wang, "Depth-resolved two-dimensional Stokes vectors of backscattered light and Mueller matrices of biological tissue measured with optical coherence tomography", *Appl. Opt*. **39**, 6318–6324 (2000).
6. S. Jiao and L.-H. V. Wang, "Two-dimensional depth-resolved Mueller matrix of biological tissue measured with double-beam polarization-sensitive optical coherence tomography", *Opt. Lett*. **27**, 101–103 (2002).
7. S. Jiao and L.-H. V. Wang, "Jones-matrix imaging of biological tissues with quadruple-channel optical coherence tomography", *J. Biomed. Opt*. **7**, 350–358 (2002).
8. Y. Yasuno, S. Makita, Y. Suto, M. Itoh, and T. Yatagai, "Birefringence imaging of human skin by polarization-sensitive spectral interferometric optical coherence tomography", *Opt. Lett*. **27**, 1803–1805 (2002)
9. S. Y. Lu and R. A. Chipman, "Homogenous and inhomogenous Jones matrix", J. Opt. Soc. Am. A **11**, 766–772 (1987).
10. C. E. Saxer, J. F. de Boer, B. H. Park, Y. Zhao, Z. Chen, and J. S. Nelson, "High-speed fiber-based polarization-sensitive optical coherence tomography of *in vivo* human skin", *Opt. Lett*. **25**, 1355–1357 (2000).